ACS NANO
Cite This: ACS Nano 2019, 13, 5421−5429
www.acsnano.org

ARTICLE

Flexible Organometal−Halide Perovskite Lasers for Speckle Reduction in Imaging Projection

Yu-Chi Wang,[†] Heng Li,[†] Yu-Heng Hong,[†] Kuo-Bin Hong,[†] Fang-Chung Chen,[†] Chia-Hung Hsu,[†,‡] Ray-Kuang Lee,[§,∥] Claudio Conti,[⊥] Tsung Sheng Kao,*[,†] and Tien-Chang Lu*[,†]

[†]Department of Photonics and Institute of Electro-Optical Engineering, College of Electrical and Computer Engineering, National Chiao Tung University, Hsinchu 30050, Taiwan

[‡]Division of Scientific Research, National Synchrotron Radiation Research Center, Hsinchu 30076, Taiwan

[§]Institute of Photonics Technologies, National Tsing Hua University, Hsinchu 30013, Taiwan

[∥]Physics Division, National Center for Theoretical Sciences, Hsinchu 30013, Taiwan

[⊥]Department of Physics, University Sapienza of Rome, Piazzale Aldo Moro 5, Rome 00185, Italy

Supporting Information

ABSTRACT: **Disorder is emerging as a strategy for fabricating random laser sources with very promising materials, such as perovskites, for which standard laser cavities are not effective or too expensive. We need, however, different fabrication protocols and technologies for reducing the laser threshold and controlling its emission. Here, we demonstrate an effectively solvent-engineered method for high-quality perovskite thin films on a flexible polyimide substrate. The fractal perovskite thin films exhibit excellent optical properties at room temperature and easily achieve lasing action without any laser cavity above room temperature with a low pumping threshold. The lasing action is also observed in curved perovskite thin films on flexible substrates. The lasing threshold can be further reduced by increasing the local curvature, which modifies the scattering strengths of the bent thin film. We also show that the curved perovskite lasers are extremely robust with respect to repeated deformations. Because of the low spatial coherence, these curved random laser devices are efficient and durable speckle-free light sources for applications in spectroscopy, bioimaging, and illumination.**

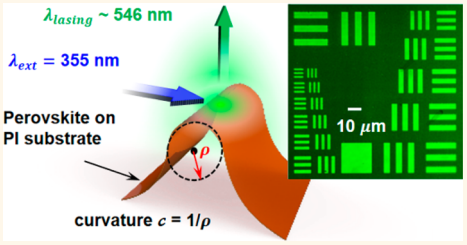

KEYWORDS: *perovskite, random laser, solvent engineering, flexible substrate, speckle-free*

Metal−halide perovskite crystalline materials have drawn significant attention due to their efficient absorption properties and high photoelectric conversion efficiency as well as their interesting optoelectronic characteristics, such as the long-range balanced electron−hole transport distances and high photoluminescence (PL) quantum efficiency over a broad wavelength range.[1−9] Moreover, the solution-processing flexibility makes them suited for advanced optoelectronic and photonic applications, particularly with respect to cost-effective and large-scale manufacturing in emerging wearable and disposable electronics.[10−12] Thus, these properties classify solution-processed organometallic−halide perovskites as promising alternative materials not only for photovoltaics applications but also for development of light-emitting devices and lasers.

Lasing with metal−halide perovskite materials has been widely studied over the past few years.[13−16] In the reported laser devices, authors employed planar polygon-shaped crystalline platelet structures with whispering gallery modes and nanowire configurations forming Fabry−Perot cavities.[15,16] Self-organized microcrystalline rod-shaped structures as waveguides and tapered fiber have been used as resonators. As such, the single-crystal configurations demonstrated the records of a low pumping threshold and a high-quality factor in the light emission performance. Authors also studied the distributed feedback Bragg (DFB) lasers with grating patterns on perovskite nanorods.[17] Their low performance in terms of thresholds is ascribed to the surface roughness of the perovskite thin films, which scatter with high loss of the laser mode in the DFB resonator. Patterned perovskite thin-film lasers with a low threshold can be also realized in a planar photonic crystal laser. Moreover, patterned and flattened perovskite layers with specific cavities can be obtained *via* the thermal nanoimprinting process.[18] The coherent light emission

Received: January 7, 2019
Accepted: April 22, 2019
Published: April 22, 2019

DOI: 10.1021/acsnano.9b00154
ACS Nano 2019, 13, 5421−5429

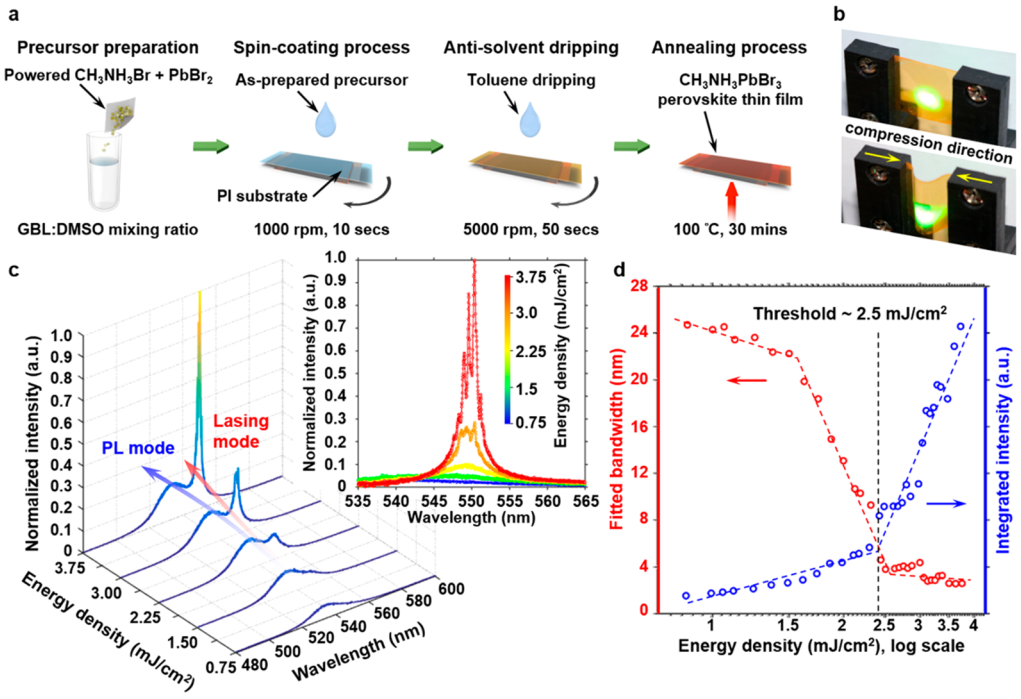

Figure 1. Optical characterizations of solvent-engineered perovskite thin films on PI substrates. (a) Schematic fabrication flow of perovskite thin films on PI substrates with a solvent-engineering process. (b) Large-scale laser light illumination from fabricated perovskite samples on flat and curved PI substrates at room temperature. (c) Power-dependent PL emission spectra of a perovskite thin film on a flat PI substrate. The peak wavelengths of the PL and lasing mode are at about 535 and 546 nm, respectively. Inset: enlarged emission spectra of the lasing mode below and above threshold of around 2.5 mJ/cm². (d) Light-out intensities and emission line widths at different pumping energy densities.

was also acquired in conformally deposited organo−halide perovskites in spherical optical cavities.[19]

All of the mentioned laser resonators require carefully engineered nanostructures, additional adhesive layer configurations, or well-controlled crystal growth. To keep the advantages of the metal−halide perovskites as proposed by the use of solution-processable optoelectronic materials with low-cost fabrication technology, it would be preferable to simplify the fabrication process as much as possible. The simplest and ultimate technological solution is removing the entire laser cavity and adopting a laser that creates its own feedback through scattering in the gain medium.[13,14,20−26] Therefore, in this report, we show a feasible route toward such an inexpensive technology by demonstrating high-performance random lasing from a solution-processed perovskite film. We study perovskite materials of methylammonium lead bromide ($CH_3NH_3PbBr_3$) by optimizing the mixing ratio of the precursor solutions to engineer the comparably reliable perovskite thin films for random lasing performance. Regarding the random lasing action from the organometallic−halide perovskite, Dhanker *et al.* first demonstrated the random lasing performance from planar organometal−$CH_3NH_3PbI_3$ perovskite microcrystal networks.[12] Soon after their discovery, we demonstrated in our previous study that the random lasing actions of solution-processed perovskites from the embedded crystalline nanostructures may be altered upon a temperature-induced phase transition.[13] Recently, several advanced studies have demonstrated that the material response and stability of perovskites can be improved by chemical anchoring or controlled in an antisolvent process.[27,28] In the case of the antisolvent dripping technique during a spin-coating process, the synthesized perovskite film generates numerous polycrystalline grains internally, and the film morphology shows almost 100% surface coverage. The pure crystal phases of each polycrystalline grain and the full surface coverage result in an outstanding power conversion efficiency of up to 22%. Here, we utilize an optimized solvent engineering process, which facilitates the synthesis of high-quality solution-processed perovskite thin films on flexible polyimide (PI) substrates. We observe the random lasing action in curved perovskite thin films on the flexible substrates above room temperature with a low threshold. Our curved perovskite random lasers exhibit low spatial coherence and excellent image quality without speckle. Considering the high durability and flexible characteristics, the proposed curved perovskite random laser is a potential speckle-free light source for future applications.

RESULTS AND DISCUSSION

The procedures involved in the antisolvent technique using a precursor solution dissolved in an engineered solvent is schematically described in Figure 1a. The engineered solvent consisted of a γ-butyrolactone (GBL) and dimethylsulfoxide (DMSO) mixture. By properly mixing the two, high-quality inorganic−organic metal−halide perovskite thin films were obtained (see Figure S1 in the Supporting Information). The antisolvent engineered perovskite thin films on the flexible PI substrates exhibit high emission efficiency, facilitating a low threshold lasing action at room temperature. Such an improvement in light emission performance may result from the compact and smooth $CH_3NH_3PbBr_3$ perovskite film fabricated with well-interconnected grain boundaries. As shown in Figure 1b, bright and uniform photoluminescence was clearly observed on the perovskite thin films on both flat and curved PI substrates which were adjusted mechanically.

DOI: 10.1021/acsnano.9b00154
ACS Nano 2019, 13, 5421−5429

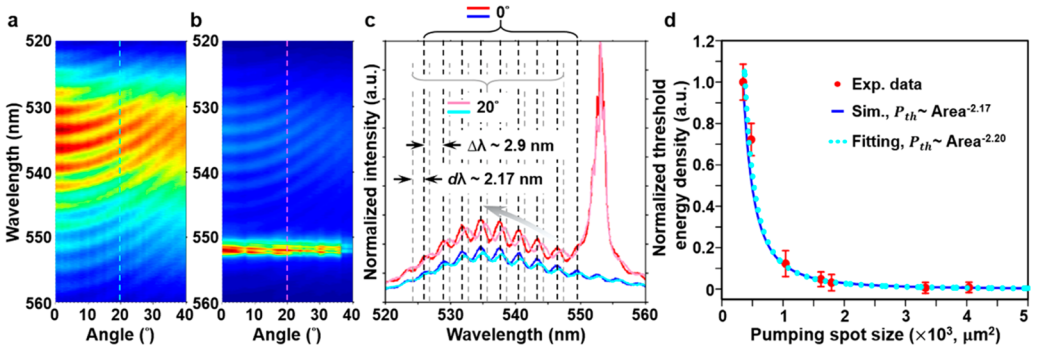

Figure 2. Far-field light emission investigation and characterization of perovskite random lasers on flat substrates. (a,b) Far-field ARPL emission spectra mappings below and beyond the lasing threshold of 2.5 mJ/cm^2. The curves in the mappings result from the interference within the Fabry−Perot cavity provided by the PI substrate. (c) Comparison of the emission spectra at normal direction and 20° detection angle for the lasing (red) and PL (blue) modes. The spacing $\Delta\lambda$ between the interference peaks is around 2.9 nm, whereas the peaks shift about 2.17 nm as the detection angle tilts 20° away from normal. (d) Threshold energy density variation with different pumping spot sizes along with simulation results. The dotted line indicates the curve fitting to the experimental data, and the solid line represents the results from theoretical calculations.

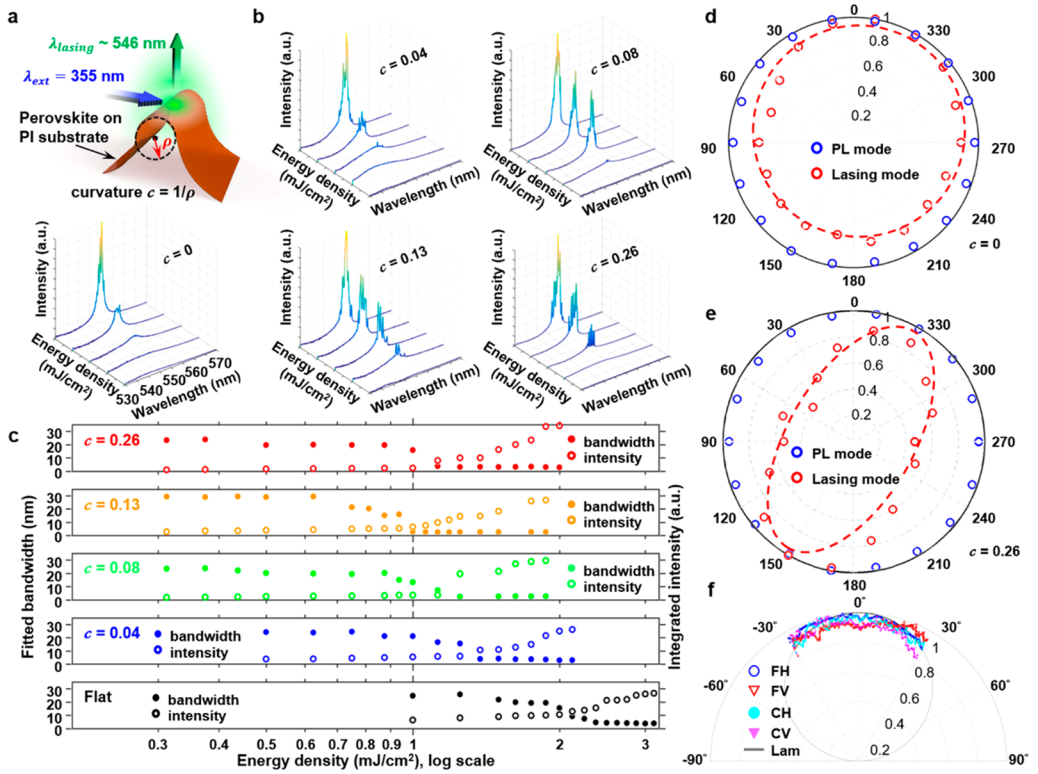

Figure 3. Perovskite random lasers on flexible substrates with varied curvatures. (a) Schematic illustration of excitation and emission of a flexible thin film perovskite laser at a bending condition. The curvature c is defined as the inverse of the radius ρ estimated from the edge of the curved PI substrate. (b) Power-dependent emission spectra of the lasing mode on flexible perovskite thin films at curvatures from flat (c = 0) to 0.26 mm^{-1}. The pumping energy densities and spectral wavelengths in all of the images are in a range from 0.5 to 2.875 mJ/cm^2 and 530 to 570 nm. (c) Light-out intensities and emission line widths at different pumping energy densities for flexible perovskite random lasers at different curvatures. The data are represented in log−linear scale. (d,e) Integrated emission intensities of perovskite thin films on flat and curved substrates (c = 0.26) at different polarization angles detected from the top of samples. (f) Divergence measurements in a range of −30 to +30° of laser light far-field intensity for four conditions: CH, curved substrate and along the curved direction; CV, curved substrate and vertical to the curved direction; FH, flat substrate and along the curved direction; FV, flat substrate and vertical to the curved direction.

We then examined the room-temperature lasing characteristics of the $CH_3NH_3PbBr_3$ perovskite samples. The power-dependent PL emission spectra of a perovskite thin film on a flat substrate are shown in Figure 1c, whereas the extracted integrated intensities and corresponding line widths of the emission peaks are plotted in the light−light (L−L) curve in a log−linear scale, as shown in Figure 1d. The PL emission spectra shown in Figure 1c are centered at approximately 535 nm below the threshold with a broad line width of around 22 nm. When the pumping energy density reached 2.5 mJ/cm^2, laser emission occurs at about 546 nm with a dramatically reduced line width down to 1.8 nm. Because there is no predefined laser cavity in the solution-processed perovskite thin film, the lasing action might originate from the random

DOI: 10.1021/acsnano.9b00154
ACS Nano 2019, 13, 5421−5429

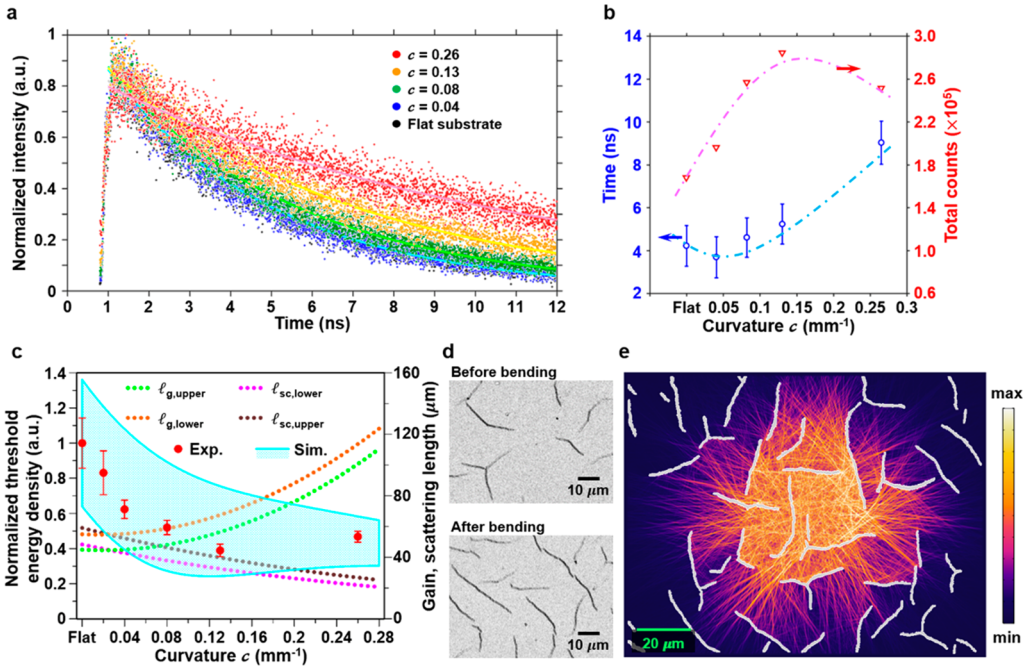

Figure 4. Characteristics of flexible thin-film perovskite random lasers. (a) Time-resolved PL traces of the perovskite thin films on the flexible substrates at different curvatures. (b) Extracted PL intensities and lifetime at different curvatures. (c) Experimental and theoretical threshold calculations of perovskite random lasers with different curvatures: l_{sc} and l_g are the scattering length and optical gain lengths as a function of curvature c, respectively. To theoretically investigate the threshold energy density, a 10% variation to the estimated l_{sc} and l_g was applied in the calculations. The dashed lines show the upper and lower bounds of the l_{sc} and l_g, respectively. The light blue region reveals simulated threshold gain values for different curvatures. (d) OM images of the perovskite sample surfaces on flat and curved substrates. (e) Calculated scattered fields on the perovskite thin film with enhanced edges above the threshold.

scattering due to the crystalline boundary or other scattering centers in the polycrystalline perovskite thin film. The details of the lasing mechanism will be discussed in the following section. At a higher optical pumping energy density above the lasing threshold, multiple lasing peaks occur, as shown in the inset of Figure 1c, which is one of the significant features of the random lasing action. The red-shifted lasing mode with respect to the PL mode is due to the lower absorption loss at the energy band tail of $CH_3NH_3PbBr_3$ perovskite.[29]

The other characteristic of the random lasing action in the perovskite thin film is observed in the angle-resolved PL (ARPL) measurements of the laser output above the perovskite film. These results are presented in Figure 2. Light radiation from the perovskite thin film below the threshold is in a wide angle from 0 to 40°, as shown in Figure 2a, where 0° represents the normal direction to the sample surface. The spontaneous emission from the perovskite film is in a broad spectral band with the central emission peak at around 535 nm. The curves in the ARPL mapping result from the interference within the Fabry−Perot cavity facilitated by the PI substrate underneath. As shown in Figure 2b, when the lasing threshold is achieved, a strong and large-angle radiation from 0 to 40° of the lasing mode is observed due to the contribution of random scattering in the perovskite thin films. We extracted the emission spectra below and above the threshold at the detection angles of 0 and 20°. The comparisons are shown in Figure 2c. The PL mode shows a regular mode spacing of around 2.9 nm, which corresponds to the thickness of the PI substrate at around 30 μm. The blue-shifted PL modes at the detection angle of 20° in comparison to those at 0° result from the phase-matching condition for the PI vertical cavity. However, the multiple lasing peaks remain at the same spectra position regardless of the detection angles, which implies that the laser action does not originate from the vertical feedback condition.

Another characteristic of the random laser action can be identified by the relationship between the laser threshold energy density and the pumping area.[12]

$$P_{th} \propto e^{-\left(\frac{\ln(A/A_0)}{G}\right)^{\lambda}} \quad (1)$$

Here, A indicates the illumination area; A_0 is the two-dimensional area occupied by a typical quasimode, and G is a parameter reflecting the disorder strength of the system. In eq 1, P_{th} is proportional to the $(A/A_0)^{1/G}$ and λ depends on the degree of disorder correlation. It has already been demonstrated that the laser threshold would decrease with an increase in the pumping area for various random laser systems, and theoretical studies on the interplay of curvature and disorder were reported.[12,30] As shown in Figure 1d, the G value is extracted to be 2.2. This dependence can be understood according to the random resonator statistical framework. As the optical pumping beam spot area decreases, the lasing threshold increases due to the smaller closed-loop path provided by the scattering effect. The lasing threshold increased rapidly, and the illumination area was less than 5×10^2 μm^2. However, when the beam spot area is larger than 2×10^3 μm^2, the lasing threshold decreases very slowly and there is almost no connection between the illumination area and the lasing threshold. This indicates that the spot size might be close to and even exceed the effective length of the scattering closed-loop. The random laser model fits quite well with the experimental results, as shown in Figure 2d.

DOI: 10.1021/acsnano.9b00154
ACS Nano 2019, 13, 5421−5429

We then demonstrate the random lasing action from curved perovskite thin films. Because the perovskite thin films were deposited on flexible PI substrates, we designed a mechanical fixture to bend the PI substrate in one direction, as shown in images of Figure 1b and the schematics of Figure 3a, in order to create curvature along one direction of the perovskite thin film for observing the structural and optical characteristics. Figure 3b shows the PL emission spectra obtained from the bending perovskite thin films at room temperature. The bending radius of the perovskite thin films includes the values of 24.6, 12.2, 7.7, and 3.8 mm corresponding to curvatures of 0.04, 0.08, 0.13, and 0.26, respectively. All bending conditions clearly show lasing action as indicated by the two-slope L−L curves and the narrowing of the line width in Figure 3c. Above the pumping threshold, multiple emission peaks can be clearly observed within an emission spectral range of 547−552 nm. When the curvature of the flexible substrate increases, the multiple lasing peaks can still be observed, with the central lasing emission peaks slightly shifted from 550 to 549 nm. The random lasing characteristics are similar to the case of the flat perovskite thin film, and it can also be validated by far-field emission, as shown in Figure 3f. The results indicate a rather large lasing divergence angle above the threshold. The far-field intensities can also be well-fitted using the Lambertian formula that exhibits characteristics of random laser emission. The far-field laser emission spectra of flat samples and others with a curvature of 0.26 were measured in both the vertical and horizontal directions with respect to the bending direction. As shown in Figure 3f, the laser emission spectra are similar for the four cases. These results demonstrate that the random laser action can be preserved even for the bending conditions. Moreover, the random lasing thresholds can be actively modulated with the bending radius. As shown in Figure 3c, the lasing threshold is reduced with an increase of the curvature. The lowest threshold was observed for the sample with a curvature of 0.13. When the curvature was increased further, the lasing threshold slightly increased. The reduction in the lasing threshold of the curved perovskite thin film will be further discussed later. It is interesting to note that the lasing mode shows a slight partially polarized emission, as shown in Figure 3d, due to the intrinsic birefringence of the PI substrate. As multiple scattered laser light will simultaneously propagate through the perovskite thin film and PI substrate, the birefringence condition of the PI substrate will affect the polarization of the laser emission. The degree of polarization is further enhanced when the PI substrate is curved due to the increased birefringence effect in the curved PI substrate, as shown in Figure 3e (related optical anisotropy investigation of the perovskite thin films on PI substrates has been carried out as shown in Figure S3 in the Supporting Information).

In order to investigate the mechanism of threshold reduction for the curved perovskite thin film, we performed time-resolved PL (TRPL) measurements. For the measured TRPL results shown in Figure 4a,b, the carrier lifetime slightly increased as the bending curvature increased from 0 to 0.15 mm^{-1}. This indicates that the luminescence efficiency slightly decreased as the curvature increased. The carrier lifetime variation might correlate to the lattice distortion of the perovskite thin film at the bending condition (see the Supporting Information for lattice measurement). However, this slight luminescence efficiency degradation cannot account for lasing threshold reduction in the curved perovskite thin film. When the curvature is beyond 0.25 mm^{-1}, the carrier lifetime suddenly increases, which significantly degrades the radiative efficiency. This observation could explain the slight increase in the lasing threshold when the curvature is very large, as shown in Figure 3c. Meanwhile, Figure 4b shows the PL emission intensity at various curvatures of the perovskite thin film. In our experimental setup, we may be able to change the curvature from flat ($c = 0$) to $c = 0.26$ mm^{-1}. Considering the lasing threshold measured in this bending range, the PL intensity increases when the curvature varies from 0 to 0.15 mm^{-1}, and this could be due to an increase in scattering, possibly as a result of the bending of the thin film. With further bending of the perovskite substrate, the PL intensity then decreased as the curvature exceeded 0.25 mm^{-1}. This response originates from the degradation of the radiative efficiency when the microscopic structural modification is too large. To identify the main scattering centers of the perovskite thin film, Figure 4d shows images of the surface morphology acquired using an optical microscope (OM) in the case of the flat and curved perovskite thin films on the PI substrate. Clear fractal edges can be observed in both samples with the enhanced contrast in the OM images. However, the fractal edges in the curved sample are more abundant and wider than those of the flat sample. This leads to a stronger scattering possibility when the traveling light interacts with the fractal edges and results in higher PL intensities when the curvature varies from 0 to 0.15 mm^{-1}. These fractal edges could also influence the random laser performance.

To investigate the threshold characteristics of the perovskite random laser, the diffusion model for light propagation in a random thin film was exploited.[12] A cavity-free laser made of a random medium can operate above a particular threshold power due to randomly scattered waves self-trapped in a closed-loop through the built-in grain boundaries. The two-dimensional diffusion model with the gain effect can be expressed as follows:[30−32]

$$\frac{\partial u(\mathbf{r}, t)}{\partial t} = D\nabla^2 u(\mathbf{r}, t) + \frac{v}{l_g} u(\mathbf{r}, t) \tag{2}$$

Here, $u(\mathbf{r},t)$ is the energy intensity, $D = vl_{sc}/2$ is the average diffusion constant, v, l_{sc}, and l_g are the transport speed of light in the medium, scattering length, and optical gain length, which are assumed to be proportional to the speed of light/n, the measured coherence length, L_c, and the carrier lifetime, respectively. The coherence length and carrier lifetime might vary with the curvature of the perovskite thin film and are obtained from the first-order spatial coherence $g^{(1)}$ and TRPL measurements, as demonstrated in Figures S4 and S5, respectively (see the Supporting Information). Here, $n = 2.21$ is the refractive index of perovskite for the lasing wavelength. To determine the threshold condition and accurately calculate the solutions of eq 2, for a stationary state, we take $u(\mathbf{r},t) = e^{-\eta v t} u(\mathbf{r})$, and it is noted that the above time-independent diffusion equation is simplified to an eigenvalue problem.

$$-\eta v u(\mathbf{r}) = \frac{vl}{2}\nabla^2 u(\mathbf{r}) + \frac{v}{l_g} u(\mathbf{r}) \tag{3}$$

As the gain is provided in the pumping area ($\pi\rho^2$), when $l_g^{-1} \neq 0$ for $|\mathbf{r}| \leq \rho$ such that $|\eta| \cong 0$, the lasing threshold condition is achieved. Figure 4e shows the calculated scattered fields above the threshold condition in the perovskite thin film due to the fractal edges. As a result, the threshold condition of the

DOI: 10.1021/acsnano.9b00154
ACS Nano 2019, 13, 5421−5429

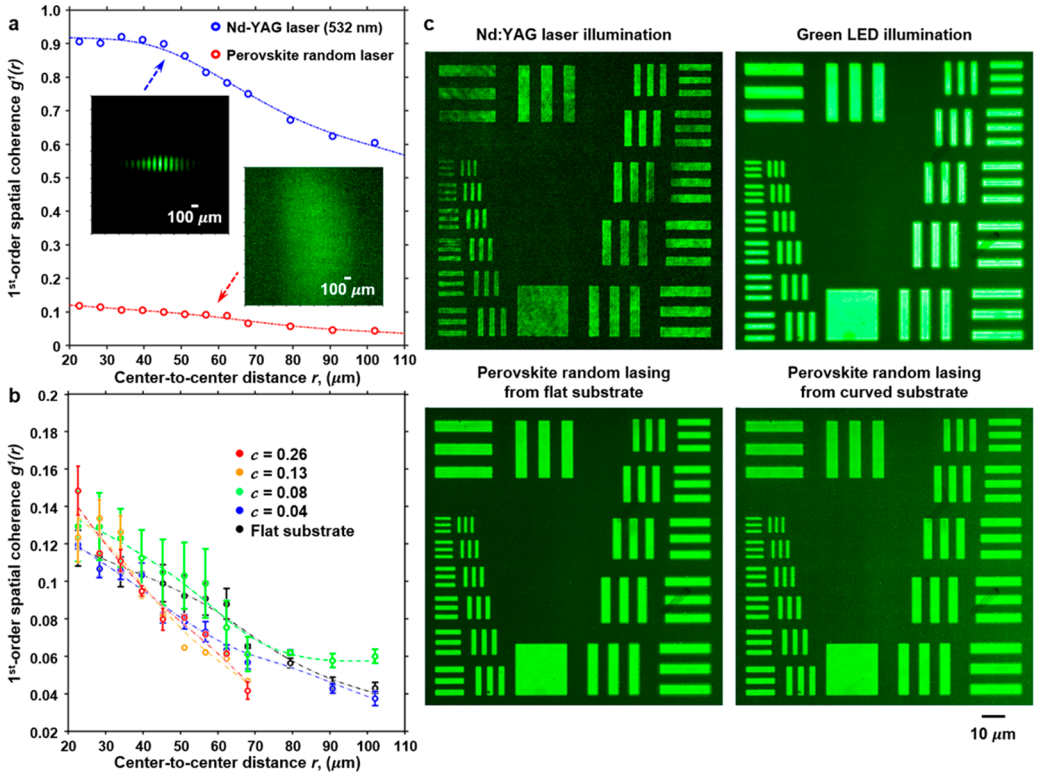

Figure 5. Optical coherence of flexible perovskite random lasers and speckle imaging. (a) Comparison of the first-order spatial coherence between the use of a conventional Nd:YAG laser and perovskite thin-film random laser as the light source in an imaging apparatus. Inset: interference patterns. (b) First-order spatial coherence of perovskite random lasers at different curvatures. (c) Optical imaging of AF resolution test chart *via* different light sources.

perovskite random laser for a variation of the pumping area can be calculated, and we can clearly observe the threshold decreases with an increase of the pumping area. There is a tendency to follow a power law with an order of −2.17, which is in very good agreement with the experimental observation represented in Figure 2d.

We also demonstrated the curvature effects on the threshold characteristics of a perovskite random laser. Figure 4c depicts the theoretical threshold conditions of perovskite random lasers with different curvatures. Multiple factors could influence the threshold condition. A strong scattering could occur when the fractal edges become more pronounced for the perovskite thin film on the curved substrates, and this could lead to a reduction of the scattering length (l_{sc}) and a corresponding reduction of the threshold. On the other hand, the increase of the gain length (l_g) as the curvature becomes larger would lead to an increase in the threshold. Therefore, there will be an optimum curvature which occurs at approximately 0.13 mm^{-1} for the lowest threshold condition for flexible perovskite random lasers.

Lasers play an important role in modern imaging systems, due to their high luminescence efficiency. However, the "speckle" that originated from the high spatial coherence of the laser light emission inevitably induces interference patterns in an imaging system, significantly degrading image quality. Random lasers with a low spatial coherence may be an innovative speckle-free intense light source for an advanced imaging apparatus. To quantitatively analyze the degree of spatial coherence and imaging capability using the perovskite random laser, tests with the Young's double slits and the 1951 U.S. Air Force (AF) resolution charts were conducted. First, light emission from perovskite thin-film random lasers was collected by a 100× objective lens and then irradiated onto double slits where the center-to-center distance, r, between the slits is varied in a range from 20 to 110 μm. The interference patterns were recorded using a charge-coupled device (CCD), whereas the first-order spatial coherence, $g^{(1)}(r)$, as a function of the separation distance could be estimated.[33−35] The interference patterns associated with a set of the double slits irradiated by a conventional laser and a perovskite random laser light source are illustrated in the insets of Figure 5a. With the acquired images, the first-order spatial coherence, $g^{(1)}(r)$, can be estimated as the results represented in Figure 5a. The values of the first-order spatial coherence in the use of the perovskite random laser light source are much lower than that in the case of the conventional laser. The maximum value of $g^{(1)}(r)$ using the perovskite random laser light source is less than 0.12, indicating low correlation between the generated light waves. After the flexible substrate is bent, the spatial coherence values are still low, as summarized in Figure 5b. The corresponding coherence lengths for the perovskite random lasers with different local curvatures can also be estimated (see Figure S5 in the Supporting Information). The variation of the coherence length as a function of the curvature indicates that the scattering effect on the perovskite surface may be altered with different bending degrees.

Figure 5c shows the illuminated images of the 1951 U.S. AF resolution test pattern using different light sources, including a Nd:YAG pulse laser, a light-emitting diode, and flat and curved perovskite random lasers. The speckle interference pattern could be observed in the image collected from the conventional Nd:YAG laser illumination. The results confirm that the

DOI: 10.1021/acsnano.9b00154
ACS Nano 2019, 13, 5421−5429

random laser could provide low spatial coherence laser output and could be highly relevant to modern imaging applications. Moreover, with the use of the perovskite random lasers, the contrast-to-noise ratio in the imaging performance can be improved, as indicated in Figure S8 in the Supporting Information. The lasing action stability of the perovskite films can be considered in the bending durability and the thermal stability, whereas the related results are presented in Figure S10 in the Supporting Information. In the bending durability test, we repeatedly bent the perovskite films on the PI substrate and measured the light emission intensity with the same pumping energy density at around 3 mJ/cm^2. After more than 2000 bending cycles, the laser light emissions still remain at similar intensities, indicating that the laser action still occurs from the perovskite thin films. Also, the thermal stability of the $MAPbBr_3$ perovskite thin films was examined with the power-dependent photoluminescence measurements. The emission intensities can be maintained as the pumping energy density below 4 mJ/cm^2. Above this pumping energy density, the emission intensity may be decreased and varied from time to time, resulting from the crystalline structure and grain boundary variations. As the pumping energy is quite high, the perovskite thin film may be damaged and cannot be recovered. Such thermally induced damage may be improved with a dielectric protecting layer coated on the top of the perovskite film. Thus, in the imaging apparatus, we carefully keep the pumping energy maintained around 3 mJ/cm^2. In our experiments, the $MAPbBr_3$ for random lasing illumination can be stable under our light irradiation condition with the maximum energy density at around 4 mJ/cm^2. The random lasing action may not only occur in the organometallic−halide perovskite thin films but also be acquired in films of colloidal cesium lead perovskite nanocrystals.[20] According to the work reported by Yakunin *et al.*, colloidal nanocrystals of cesium lead perovskite $CsPbX_3$ (X = Cl, Br, or I, or mixed Cl/Br and Br/I systems) also exhibit low threshold amplified spontaneous emission and similar lasing action from the random scattering in films of $CsPbX_3$ nanocrystals. Thus, we believe that the similar lasing behavior can be acquired within different types or various composites of perovskites.

From an application perspective, the electrical pumping scheme is very important and also a great challenge for making random laser devices practical. The electrically pumped random laser may be achieved *via* the effective external injection of electrons and holes or the random cavities with hybrid p-i-n and metal−insulator−semiconductor structures.[36] Although hybrid perovskites are recently considered as promising emitter materials due to their attractive properties, there are still many challenges remaining in the development of electrically pumped perovskite-based light-emitting devices such as the choice of electron- and hole-transport matching layers for higher injection current densities and also the thermal stability for lower heating effect.[37] With the improved material properties and properly integrated configurations, the intrinsic grains and voids in perovskite thin films may support the strong optical scattering, achieving electrically pumped lasing devices. Moreover, hybrid halide perovskites are applicable for emission wavelength tuning by changing their structures and morphology with a variety of shapes and sizes during synthesis. With the variation of anions and cations in perovskite fabrication, the photoluminescence emissions may cover a side color gamut. In this paper, we have demonstrated that the high-quality $MAPbBr_3$ perovskite thin films can be prepared by an optimized antisolvent process with a proper mixture of precursors. With the solvent-engineering process, one may expect that quality-improved perovskites with different halide compositions or partial halide substitution can be acquired to realize other component random lasers at different colors.

CONCLUSIONS

In conclusion, we have demonstrated low-cost solution-processed perovskite random lasers on flexible PI substrates. An optimized solvent-engineered method is developed to obtain organometallic−halide perovskite thin films with promising optical performance that facilitate low threshold random lasing action at room temperature. The perovskite thin film on the flexible substrate can be further curved to achieve even lower lasing threshold operation due to a stronger scattering effect caused by the grain boundaries in the fractal perovskite thin film. The curved perovskite random lasers operated at the green wavelength band demonstrated low spatial coherence and facilitated imaging capability with low speckle. Considering the highly durable and flexible characteristics, the proposed flexible perovskite random laser is a potential speckle-free light source with numerous applications for laser projection and image processing.

METHODS

Sample Preparation. As shown in Figure 1a, first, the powdered lead(II) bromide ($PbBr_2$) and methylammonium bromide (MABr) were included into an engineered solvent and kept stirring until completely dissolved, turning into a transparent precursor solution with 1 M concentration. Next, the as-prepared precursor solution was deposited onto UV-O_3-cleaned PI substrates by a consecutive two-stage spin-coating process at 1000 and 5000 rpm for 10 and 50 s, respectively. Because the PI substrate is highly flexible, it is taped on a glass substrate to prevent wrinkling while spin-coating. During the second spin-coating stage, a drop of antisolvent toluene was continuously dripped onto the glass substrates. Finally, the resulting thin films were annealed at 100 °C for 30 min to remove the residual solvents and transit the intermediate solvate phase into the perovskite, generating the orange and bright lead bromide perovskite films. All of the fabrications were done inside a nitrogen-filled glovebox at room temperature. The perovskite thin film on the PI flexible substrate was then detached from the glass substrate to be tested at room temperature.

Micro-PL Measurement. The power-dependent PL measurements were conducted using a third harmonic generation of a Nd:YVO_4 pulse laser as an optical excitation source of 355 nm, whereas the pulse duration and the repetition rate were 0.5 ns and 1 kHz, respectively. By launching the laser light beam into 0.55 NA microscope objective lens, the focal spot size can be concentrated at around 70 μm in diameter, irradiating on the perovskite sample surface. Light emitted from the perovskites was collected by the same objective lens and transmitted through a UV optical fiber into a monochromator (Horiba iHR320) with a spectral resolution of 0.2 nm, together with a nitrogen-cooled CCD, recording the PL emission spectra at different characteristic excitation powers. For the polarization measurement, there is a polarizer before the fiber. That 90° polarizer angle is defined to be perpendicular to the bending direction.

Angle-Resolved PL Measurements. ARPL measurements were carried out with the same 355 nm pulse laser with the maximum oblique incident angle up to 40°. The emitted light was collected by a UV optical fiber with a 600 μm core mounted on a rotating stage with an angular resolution of 1° and detected by a nitrogen-cooled CCD attached to the monochromator.

DOI: 10.1021/acsnano.9b00154
ACS Nano 2019, 13, 5421−5429

ASSOCIATED CONTENT

Supporting Information

The Supporting Information is available free of charge on the ACS Publications website at DOI: 10.1021/acsnano.9b00154.

Morphology of solution-processed perovskite thin films fabricated at different precursor ratios; structural configurations of perovskite films at different curvatures; birefringence investigation of the PI substrate; estimation of the optical gain lengths and scattering lengths from experimental measurements; experimental setups of the angle-resolved photoluminescence measurements, Young's double slit interference measurements, and imaging projection of the AF test charts; comparison of the derived contrast-to-noise ratios; reliability tests (PDF)

AUTHOR INFORMATION

Corresponding Authors

*E-mail: tskao@nctu.edu.tw.
*E-mail: timtclu@mail.nctu.edu.tw.

ORCID

Heng Li: 0000-0001-5276-1846
Kuo-Bin Hong: 0000-0001-5027-6273
Tsung Sheng Kao: 0000-0001-5292-9717

Author Contributions

T.S.K. and T.-C.L. initiated the study. Y.-C.W., Y.-H.H., and F.-C.C. designed and prepared the samples. Y.-C.W. and H.L. performed the optical characterizations. C.-H.H. performed the crystalline analysis. K.-B.H., R.-K.L., and C.C. performed the numerical simulation and modeling. Y.-C.W., K.-B.H, T.S.K., and T.-C.L. wrote the manuscript. Y.-C.W., H.L., and Y.-H.H. equally contributed to this work. All authors discussed the results and commented on the manuscript.

Notes

The authors declare no competing financial interest.

ACKNOWLEDGMENTS

This work was, in part, financially supported by the Research Team of Photonic Technologies and Intelligent Systems at NCTU within the framework of the Higher Education Sprout Project by the Ministry of Education (MOE) in Taiwan and also partially supported by Minister of Science and Technology (MOST) under Contract Nos. MOST 107-2119-M-009-016 and MOST 107-2221-E-009-116-MY3.

REFERENCES

(1) Green, M. A.; Ho-Baillie, A.; Snaith, H. J. The Emergence of Perovskite Solar Cells. *Nat. Photonics* **2014**, *8*, 506−514.

(2) Stranks, S. D.; Eperon, G. E.; Grancini, G.; Menelaou, C.; Alcocer, M. J. P.; Leijtens, T.; Herz, L. M.; Petrozza, A.; Snaith, H. J. Electron-Hole Diffusion Lengths Exceeding 1 Micrometer in an Organometal Trihalide Perovskite Absorber. *Science* **2013**, *342*, 341−344.

(3) Xing, G.; Mathews, N.; Sun, S.; Lim, S. S.; Lam, Y. M.; Gratzel, M.; Mhaisalkar, S.; Sum, T. C. Long-Range Balanced Electron- and Hole-Transport Lengths in Organic-Inorganic $CH_3NH_3PbI_3$. *Science* **2013**, *342*, 344−347.

(4) Yang, W. S.; Park, B.-W.; Jung, E. H.; Jeon, N. J.; Kim, Y. C.; Lee, D. U.; Shin, S. S.; Seo, J.; Kim, E. K.; Noh, J. H.; Seok, S. I. Iodide Management in Formamidinium-Lead-Halide-Based Perovskite Layers for Efficient Solar Cells. *Science* **2017**, *356*, 1376−1379.

(5) Cheng, P.; Xu, Z.; Li, J.; Liu, Y.; Fan, Y.; Yu, L.; Smilgies, D.-M.; Müller, C.; Zhao, K.; Liu, S. F. Highly Efficient Ruddlesden-Popper Halide Perovskite $PA_2MA_4Pb_5I_{16}$ Solar Cells. *ACS Energy Lett.* **2018**, *3*, 1975−1982.

(6) Guo, Z.; Wan, Y.; Yang, M.; Snaider, J.; Zhu, K.; Huang, L. Long-Range Hot-Carrier Transport in Hybrid Perovskites Visualized by Ultrafast Microscopy. *Science* **2017**, *356*, 59−62.

(7) Zhou, H.; Chen, Q.; Li, G.; Luo, S.; Song, T.-B.; Duan, H.-S.; Hong, Z.; You, J.; Liu, Y.; Yang, Y. Interface Engineering of Highly Efficient Perovskite Solar Cells. *Science* **2014**, *345*, 542−546.

(8) Xing, G.; Mathews, N.; Lim, S. S.; Yantara, N.; Liu, X.; Sabba, D.; Gratzel, M.; Mhaisalkar, S.; Sum, T. C. Low-Temperature Solution-Processed Wavelength-Tunable Perovskites for Lasing. *Nat. Mater.* **2014**, *13*, 476−480.

(9) Tan, Z.-K.; Moghaddam, R. S.; Lai, M.-L.; Docampo, P.; Higler, R.; Deschler, F.; Price, M.; Sadhanala, A.; Pazos, L. M.; Credgington, D.; Hanusch, F.; Bein, T.; Snaith, H. J.; Friend, R. H. Bright Light-Emitting Diodes Based on Organometal Halide Perovskite. *Nat. Nanotechnol.* **2014**, *9*, 687−692.

(10) Protesescu, L.; Yakunin, S.; Bodnarchuk, M. I.; Krieg, F.; Caputo, R.; Hendon, C. H.; Yang, R. X.; Walsh, A.; Kovalenko, M. V. Nanocrystals of Cesium Lead Halide Perovskites ($CsPbX_3$, X = Cl, Br, and I): Novel Optoelectronic Materials Showing Bright Emission with Wide Color Gamut. *Nano Lett.* **2015**, *15*, 3692−3696.

(11) Peng, X.; Yuan, J.; Shen, S.; Gao, M.; Chesman, A. S. R.; Yin, H.; Cheng, J.; Zhang, Q.; Angmo, D. Perovskite and Organic Solar Cells Fabricated by Inkjet Printing: Progress and Prospects. *Adv. Funct. Mater.* **2017**, *27*, 1703704.

(12) Dhanker, R.; Brigeman, A. N.; Larsen, A. V.; Stewart, R. J.; Asbury, J. B.; Giebink, N. C. Random Lasing in Organo-Lead Halide Perovskite Microcrystal Networks. *Appl. Phys. Lett.* **2014**, *105*, 151112.

(13) Kao, T. S.; Chou, Y.-H.; Chou, C.-H.; Chen, F.-C.; Lu, T.-C. Lasing Behaviors upon Phase Transition in Solution-Processed Perovskite Thin Films. *Appl. Phys. Lett.* **2014**, *105*, 231108.

(14) Zhang, Q.; Ha, S. T.; Liu, X.; Sum, T. C.; Xiong, Q. Room-Temperature Near-Infrared High-Q Perovskite Whispering-Gallery Planar Nanolasers. *Nano Lett.* **2014**, *14*, 5995−6001.

(15) Zhu, H.; Fu, Y.; Meng, F.; Wu, X.; Gong, Z.; Ding, Q.; Gustafsson, M. V.; Tuan Trinh, M.; Jin, S.; Zhu, X.-Y. Lead Halide Perovskite Nanowire Lasers with Low Lasing Thresholds and High Quality Factors. *Nat. Mater.* **2015**, *14*, 636−642.

(16) Mi, Y.; Liu, Z.; Shang, Q.; Niu, X.; Shi, J.; Zhang, S.; Chen, J.; Du, W.; Wu, Z.; Wang, R.; Qiu, X.; Hu, X.; Zhang, Q.; Wu, T.; Liu, X. Fabry−Pérot Oscillation and Room Temperature Lasing in Perovskite Cube-Corner Pyramid Cavities. *Small* **2018**, *14*, 1703136.

(17) Jia, Y.; Kerner, R. A.; Grede, A. J.; Brigeman, A. N.; Rand, B. P.; Giebink, N. C. Diode-Pumped Organo-Lead Halide Perovskite Lasing in a Metal-Clad Distributed Feedback Resonator. *Nano Lett.* **2016**, *16*, 4624−4629.

(18) Chen, S.; Roh, K.; Lee, J.; Chong, W. K.; Lu, Y.; Mathews, N.; Sum, T. C.; Nurmikko, A. A Photonic Crystal Laser from Solution Based Organo-Lead Iodide Perovskite Thin Films. *ACS Nano* **2016**, *10*, 3959−3967.

(19) Sutherland, B. R.; Hoogland, S.; Adachi, M. M.; Wong, C. T. O.; Sargent, E. H. Conformal Organohalide Perovskites Enable Lasing on Spherical Resonators. *ACS Nano* **2014**, *8*, 10947−10952.

(20) Yakunin, S.; Protesescu, L.; Krieg, F.; Bodnarchuk, M. I.; Nedelcu, G.; Humer, M.; De Luca, G.; Fiebig, M.; Heiss, W.; Kovalenko, M. V. Low-Threshold Amplified Spontaneous Emission and Lasing from Colloidal Nanocrystals of Caesium Lead Halide Perovskites. *Nat. Commun.* **2015**, *6*, 8056.

(21) Shi, Z.-F.; Sun, X.-G.; Wu, D.; Xu, T.-T.; Tian, Y.-T.; Zhang, Y.-T.; Li, X.-J.; Du, G.-T. Near-Infrared Random Lasing Realized in a Perovskite $CH_3NH_3PbI_3$ Thin Film. *J. Mater. Chem. C* **2016**, *4*, 8373−8379.

(22) Liu, S.; Sun, W.; Li, J.; Gu, Z.; Wang, K.; Xiao, S.; Song, Q. Random Lasing Actions in Self-Assembled Perovskite Nanoparticles. *Opt. Eng.* **2016**, *55*, 057102.

DOI: 10.1021/acsnano.9b00154
ACS Nano 2019, 13, 5421−5429

(23) Li, X.; Wang, Y.; Sun, H.; Zeng, H. Amino-Mediated Anchoring Perovskite Quantum Dots for Stable and Low-Threshold Random Lasing. *Adv. Mater.* **2017**, *29*, 1701185.
(24) Yuan, S.; Chen, D.; Li, X.; Zhong, J.; Xu, X. *In Situ* Crystallization Synthesis of $CsPbBr_3$ Perovskite Quantum Dot-Embedded Glasses with Improved Stability for Solid-State Lighting and Random Upconverted Lasing. *ACS Appl. Mater. Interfaces* **2018**, *10*, 18918−18926.
(25) Safdar, A.; Wang, Y.; Krauss, T. F. Random Lasing in Uniform Perovskite Thin Films. *Opt. Express* **2018**, *26*, A75−A84.
(26) Ghofraniha, N.; Viola, I.; Di Maria, F.; Barbarella, G.; Gigli, G.; Conti, C. Random Laser from Engineered Nanostructures Obtained by Surface Tension Driven Lithography. *Laser Photonics Rev.* **2013**, *7*, 432−438.
(27) Li, Y.; Wang, J.; Yuan, Y.; Dong, X.; Wang, P. Anti-Solvent Dependent Device Performance in $CH_3NH_3PbI_3$solar Cells: The Role of Intermediate Phase Content in the As-Prepared Thin Films. *Sustainable Energy Fuels* **2017**, *1*, 1041−1048.
(28) Guo, Y.; Ma, J.; Lei, H.; Yao, F.; Li, B.; Xiong, L.; Fang, G. Enhanced Performance of Perovskite Solar Cells *via* Anti-Solvent Nonfullerene Lewis Base IT-4F Induced Trap-Passivation. *J. Mater. Chem. A* **2018**, *6*, 5919−5925.
(29) Fang, H. H.; Adjokatse, S.; Shao, S.; Even, J.; Loi, M. A. Long-Lived Hot-Carrier Light Emission and Large Blue Shift in Formamidinium Tin Triiodide Perovskites. *Nat. Commun.* **2018**, *9*, 243.
(30) Ghofraniha, N.; Viola, I.; Zacheo, A.; Arima, V.; Gigli, G.; Conti, C. Transition from Nonresonant to Resonant Random Lasers by the Geometrical Confinement of Disorder. *Opt. Lett.* **2013**, *38*, 5043−5046.
(31) Letokhov, V. S. Generation of Light by a Scattering Medium with Negative Resonance Absorption. *Sov. Phys. JETP* **1968**, *26*, 835−840.
(32) Cao, H. Lasing in Random Media. *Waves Random Media* **2003**, *13*, R1−R39.
(33) Brittman, S.; Garnett, E. C. Measuring *n* and *k* at the Microscale in Single Crystals of $CH_3NH_3PbBr_3$ Perovskite. *J. Phys. Chem. C* **2016**, *120*, 616−620.
(34) Redding, B.; Choma, M. A.; Cao, H. Speckle-Free Laser Imaging Using Random Laser Illumination. *Nat. Photonics* **2012**, *6*, 355−359.
(35) Deng, H.; Solomon, G. S.; Hey, R.; Ploog, K. H.; Yamamoto, Y. Spatial Coherence of a Polariton Condensate. *Phys. Rev. Lett.* **2007**, *99*, 126403.
(36) Yu, S. F. Electrically Pumped Random Lasers. *J. Phys. D: Appl. Phys.* **2015**, *48*, 483001.
(37) Veldhuis, S. A.; Boix, P. P.; Yantara, N.; Li, M.; Sum, T. C.; Mathews, N.; Mhaisalkar, S. G. Perovskite Materials for Light-Emitting Diodes and Lasers. *Adv. Mater.* **2016**, *28*, 6804−6834.

DOI: 10.1021/acsnano.9b00154
ACS Nano 2019, 13, 5421−5429